ORGANOMETALLICS

Article

pubs.acs.org/Organometallics

DFT and Experimental Studies on the PtX_2/X^--Catalyzed Olefin Hydroamination: Effect of Halogen, Amine Basicity, and Olefin on Activity, Regioselectivity, and Catalyst Deactivation

Pavel A. Dub,[†] Aurélien Béthegnies,[†] and Rinaldo Poli*[,†,‡]

[†]CNRS, LCC (Laboratoire de Chimie de Coordination), Université de Toulouse, UPS, INP, 205, route de Narbonne, F-31077 Toulouse, France

[‡]Institut Universitaire de France, 103, bd Saint-Michel, 75005 Paris, France

Supporting Information

ABSTRACT: A DFT/B3LYP study with inclusion of solvent and temperature effects has probed the olefin activation mechanism for the intermolecular hydroamination of ethylene and 1-hexene by aniline derivatives catalyzed by the PtX_2/X^- system on the basis of a variety of experimental results, including new experiments on catalyst deactivation. For ethylene and aniline, the calculated $\Delta G^{\ddagger}_{cycle}$ between the resting state $[PtX_3(C_2H_4)]^-$, $\mathbf{1}^X$, and the TOF-determining transition state of the C−H reductive elimination from $[PtX_3(H)(CH_2CH_2NHPh)]^-$, $\mathbf{TS2}^X$, is slightly smaller for X = Br than for Cl or I. The $\Delta G^{\ddagger}_{cycle}$ decreases as the aniline basicity decreases. For the slightly less efficient hydroamination of 1-hexene, $\Delta G^{\ddagger}_{cycle}$ is greater than that for the hydroamination of ethylene, with a preference for the Markovnikov addition, in agreement with experiment and with essentially equivalent $\Delta G^{\ddagger}_{cycle}$ values for the Br and I systems. In general, the results of the calculations are in agreement with the experimental observation. A clear-cut comparison of trends is hampered by the small energy differences and by the possibility, proven in certain cases, that the reaction parameters under investigation affect the catalyst degradation rate in addition to its intrinsic activity. Extrapolation of the computational study to the fluoride system suggests that this should be even more active. However, experimental studies show that this is not the case. The reason for this anomaly has been traced to the basicity of the fluoride ion, which triggers more rapid catalyst decomposition. A bonding analysis of $\mathbf{1}^X$ indicates a significant push−pull π interaction between the C_2H_4 and the *trans*-F ligand.

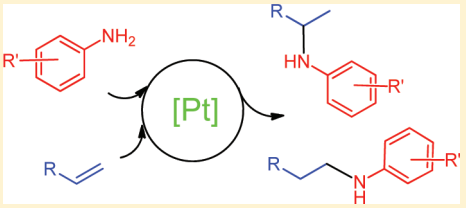

1. INTRODUCTION

Hydroamination, the direct addition of an amine N−H bond across an unsaturated C−C bond, is a challenging transformation for which catalytic approaches are attracting much interest in both academia and industry worldwide.[1] Alkenes are the most difficult substrates to hydroaminate,[2] especially for the intermolecular version and when using nonactivated substrates, namely, the simple α-olefins.[3] An additional challenge concerns the N−H addition regiochemistry in favor of the anti-Markovnikov product for monosubstituted olefins,[4] listed as one of the "Ten Challenges for Catalysis".[2] For the homogeneously catalyzed hydroamination of ethylene and other nonactivated olefins, limited success was achieved by using Li,[5] lanthanides,[6,7] Zr,[8] and late transition metals, such as Fe,[9] Ru,[10−12] Rh,[13−15] Ir,[14,15] Pd,[16,17] Ag,[18] Au,[19−22] and notably Pt.[23−25]

Investigations initiated in our team by J.-J. Brunet have shown that the hydroamination of ethylene or 1-hexene by anilines is catalyzed by PtX_2 in the presence of $^nBu_4PX$ (X = Cl, Br, I) as an activator, this being one of the most efficient catalytic systems reported for this challenging transformation.[26−29] The hydroamination catalytic activity is slightly lower for 1-hexene than for ethylene under the same conditions. The highest productivity (expressed by the turnover number, TON) in the hydroamination of ethylene was obtained with the catalyst $PtBr_2/nBu_4PBr$, whereas hydroamination of 1-hexene is most productive with $PtBr_2/nBu_4PI$,[29] an observation that has not yet been rationalized. Halide ion effects have also been observed for other types of catalyzed transformations, but poorly understood in most cases.[30−33] Another interesting observation, made for the hydroamination of ethylene, is that the TON is inversely proportional to the $ArNH_2$ basicity.[26] A greater productivity for less basic amines (anilines, carboxamides, and sulfonamides) has also been reported for the intermolecular hydroamination of ethylene catalyzed by other Pt systems, notably $PtCl_2(C_2H_4)_2$[23] and $Pt(COD)(OTf)_2$.[24] Finally, a high Markovnikov selectivity (95%) is observed for the 1-hexene hydroamination.[27]

The hydroamination reaction with late-transition-metal complexes as catalysts can, in principle, follow an olefin activation or an amine activation mechanism, and the former appears as the most likely option on the basis of experimental evidence for group 10 metals.[29] The mechanism has been analyzed by a few computational investigations. Restricting the citations to the intermolecular version and to late-transition-

Received: September 29, 2011
Published: December 6, 2011

   dx.doi.org/10.1021/om2009149 | *Organometallics* 2012, 31, 294−305

metal catalysts, a first report by Senn et al. addressed the model NH_3 addition to ethylene catalyzed by the $[MCl(PH_3)(C_2H_4)]^{z+}$ complexes of group 9 (z = 0) and 10 (z = 1) metals.[34] The study addressed only the olefin activation pathway for the group 10 metals and showed that the TOF-determining step is the H−$CH_2CH_2NH_2$ bond formation by reductive elimination from a Pt^{IV} aminoalkyl hydride intermediate, whereas the NH_3 nucleophilic addition to the activated ethylene is thermodynamically and kinetically favorable. More recently, Tsipis and Kefalidis, using the "Pt^0" model complex $Pt(C_2H_4)(PH_3)$, explored only the amine activation pathway, finding the reaction to be limited by the product reductive elimination step from the Pt^{II} amido alkyl intermediate.[35] Other computational studies (e.g., on gold-catalyzed diene[36] or ethylene[37] hydroamination or palladium-catalyzed vinylarenes hydroamination[38]) have also explored solely the olefin activation mechanism.

In a recent article, we have reported a detailed DFT analysis of the catalytic cycle for the C_2H_4/$PhNH_2$ reaction catalyzed by the $PtBr_2/Br^-$ system.[39] This study indicated that the preferred pathway is the olefin activation, rather than the amine activation. The best pathway, shown schematically in Scheme 1, involves bromide and olefin coordination to give the resting-state complex $[PtBr_3(C_2H_4)]^-$ ($\mathbf{1}^{Br}$). Other off-loop species, namely, *trans*-$PtBr_2(C_2H_4)(PhNH_2)$ ($\mathbf{2}^{Br}$), *cis*-$PtBr_2(C_2H_4)(PhNH_2)$, *trans*- and *cis*-$PtBr_2(C_2H_4)_2$, and *trans*-$PtBr_2(PhNH_2)_2$ ($\mathbf{3}^{Br}$) were also found at relatively low energy (in agreement with experimental equilibrium studies),[40] the lowest ones being $\mathbf{2}^{Br}$ and $\mathbf{3}^{Br}$.

Scheme 1. Mechanism of the $PtBr_2/Br^-$-Catalyzed Hydroamination of C_2H_2 by Aniline[39]

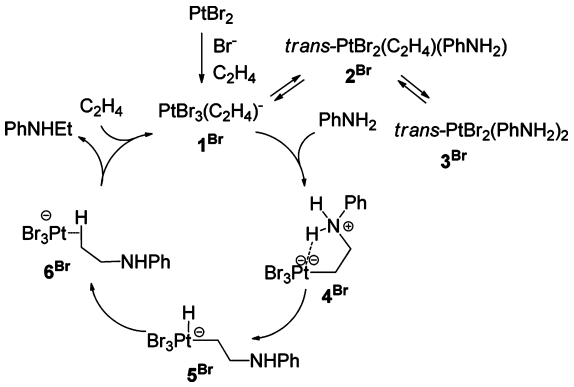

The essential features of the catalytic cycle are also shown as an energetic profile in Figure 1. The aniline nucleophilic addition to $\mathbf{1}^{Br}$ yields the zwitterionic complex $[PtBr_3(CH_2CH_2NH_2Ph)]^-$ ($\mathbf{4}^{Br}$) through the transition state $\mathbf{TS1}^{Br}$. Although the nucleophilic addition to other olefin complexes, notably $\mathbf{2}^{Br}$ and *trans*-$PtBr_2(C_2H_4)_2$, has a lower barrier, only $\mathbf{4}^{Br}$ is the productive intermediate. The latter easily transfers a proton to the Pt atom to yield $[PtHBr_3(CH_2CH_2NHPh)]^-$ ($\mathbf{5}^{Br}$), which then proceeds to C−H reductive elimination through the TOF-determining transition state $\mathbf{TS2}^{Br}$ with formation of the transient σ-complex $[PtBr_3(k^2\text{:}C,H\text{-}HCH_2CH_2NHPh)]^-$ ($\mathbf{6}^{Br}$). Liberation of the product from $\mathbf{6}^{Br}$ (or from a rearranged isomeric form with an N-bonded hydroamination product, $[PtBr_3(NHEtPh)]^-$, $\mathbf{7}^{Br}$) via ligand substitution by a new C_2H_4 molecule regenerates $\mathbf{1}^{Br}$. The overall activation barrier is determined by the free energy difference ($\Delta G^{\ddagger}_{cycle}$) between the resting state and the TOF-determining transition state,[41,42] which are, respectively, $\mathbf{1}^{Br}$ and $\mathbf{TS2}^{Br}$.

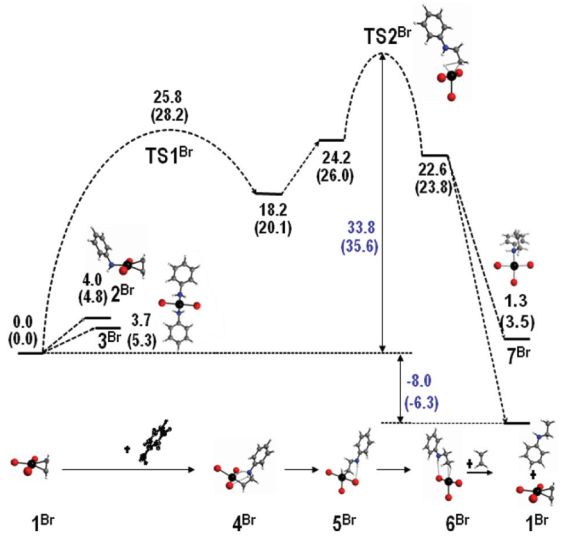

Figure 1. Free energy profile of the aniline addition to ethylene catalyzed by $PtBr_2/Br^-$.[39] Values are ΔG^{CPCM} (aniline) relative to $[PtBr_3(C_2H_4)]^-$ in kcal mol^{-1} at 298.15 K (and at 423.15 K in parentheses).

The aim of this article is to test the proposed catalytic cycle, by means of additional DFT investigations, to check whether it fits with the other observations highlighted above, and to possibly provide their rationalization. Additional catalytic experiments have also been carried out, showing how the observed TON is a reflection not only of the catalytic activity (TOF, related to the $\Delta G^{\ddagger}_{cycle}$) but also of catalyst decomposition, which has been traced to the decomposition of the zwitterionic intermediate (**4**), by reaction with an external base.

2. RESULTS AND DISCUSSION

As mentioned in the Introduction, the prototypical hydroamination process investigated in our laboratory has been the addition of aniline to ethylene, for which the highest TONs were found for the PtX_2/X^- catalytic system with X = Br. Therefore, the previously reported comprehensive computational study of the catalytic cycle was restricted to this halide and to ethylene as the olefin and aniline as the amine.[39] The $\Delta G^{\ddagger}_{cycle}$ value resulting from the study (35.6 kcal mol^{-1}) is in relatively good agreement, given the computational approximations, with the experimentally measured catalytic turnover frequency (38 h^{-1} at 150 °C,[26] which yields the upper estimate of 28.9 kcal/mol). The discrepancy between the calculation and the experiment (ca. 7 kcal mol^{-1}) is not unreasonable given the usual precision of the DFT method, considering the additional approximation involved in modeling solvation effects for ionic species and the estimation of thermodynamic parameters in a condensed phase.[43] For comparison purposes, the additional calculations presented in this contribution were carried out at the same level of theory, with inclusion of the gas-phase free energy and solvent effects at the CPCM level in aniline, but without consideration of ion-pairing effects. The reasons for these choices have been discussed previously.[39,40,43]

a. Halide Effect in the Hydroamination of Ethylene.

All energies are given with respect to the reference complex

dx.doi.org/10.1021/om2009149 | *Organometallics* 2012, 31, 294−305

$[PtX_3(C_2H_4)]^-$, $\mathbf{1}^X$, taking into account the values of all the species that are added to or subtracted from the system. The results are shown in Figure 2. As mentioned above, the

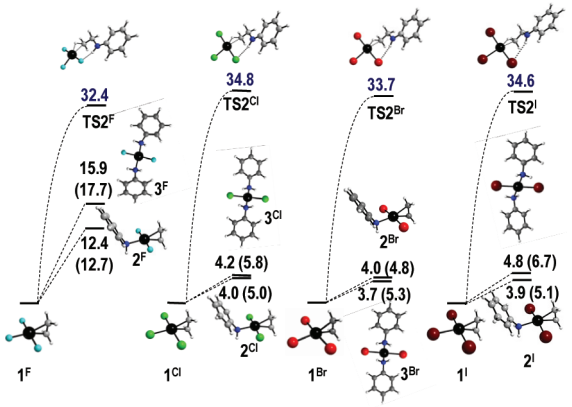

Figure 2. Relative Gibbs free energies of $[PtX_3(C_2H_4)]^-$ ($\mathbf{1}^X$), *trans*-$PtX_2(C_2H_4)(PhNH_2)$ ($\mathbf{2}^X$), *trans*-$PtX_2(PhNH_2)_2$ ($\mathbf{3}^X$), and the TOF-determining transition state ($\mathbf{TS2}^X$) for the ethylene/aniline process. Values are ΔG^{CPCM} (aniline) relative to $\mathbf{1}^X$ in kcal mol^{-1} at 298.15 K (and at 423.15 K in parentheses).

previously reported investigation had shown that complex $\mathbf{1}^{Br}$ is the catalyst resting state for the X = Br system.[39] The next-lowest ethylene-containing system was found to be *trans*-$PtBr_2(C_2H_4)(PhNH_2)$, $\mathbf{2}^{Br}$, only 4.0 kcal mol^{-1} higher than the resting state, whereas *trans*-$PtBr_2(PhNH_2)_2$ ($\mathbf{3}^{Br}$) is even closer at +3.6 kcal mol^{-1}. Because the effect of X on the relative energy of compounds $\mathbf{1}^X$, $\mathbf{2}^X$, and $\mathbf{3}^X$ could not be predicted a priori, we have also run calculations of all systems $\mathbf{2}^X$ and $\mathbf{3}^X$ to ensure that we always consider the correct form of the resting state. As shown in Figure 2, the lowest-energy species is, in each case, complex $\mathbf{1}^X$, and this remains true at 150 °C (catalytic conditions) according to the calculations. Other potential off-loop intermediates, obtained by ligand-exchange processes from $\mathbf{1}^X$ with the molecules present under catalytic conditions (X^-, aniline, and ethylene), were at even greater energy for X = Br,[43] and their optimization for the other halogen systems was not pursued.

The energy gap between $\mathbf{1}^X$ and complexes $\mathbf{2}^X$ and $\mathbf{3}^X$ is much greater for X = F (12.4 kcal/mol for $\mathbf{2}^F$ and 15.9 kcal/mol for $\mathbf{3}^F$), lower and relatively halogen-independent for the three heavier halogens (ca. 4 kcal/mol for both series). Although this has no relevance to the catalyst activity, since the resting state remains, in all cases, the $\mathbf{1}^X$ system, it is interesting to understand this "fluoride effect". With this objective, we have carried out more detailed analyses of the electronic structure and charge distribution for the $\mathbf{1}^X$, $\mathbf{2}^X$, and $\mathbf{3}^X$ complexes, and the most relevant results are shown in Table 1.

As the halogen becomes less electronegative, the halogen atom natural charge predictably changes to less negative values for all series of complexes. The metal charge changes even more dramatically (for instance, from 1.022 for $\mathbf{1}^F$ to −0.251 for $\mathbf{1}^I$, a change of more than 1 unit). Counterintuitively, the ethylene C atoms in the $\mathbf{1}^X$ and $\mathbf{2}^X$ series are more negatively charged in the systems with the more electronegative halogen atoms, where the metal is more positively charged. The change is particularly pronounced on going from F to Cl and greater for the $\mathbf{1}^X$ system (+0.041) than for the $\mathbf{2}^X$ system (+0.021). This suggests that there is greater metal−ethylene back-bonding, yielding greater contribution of the platinacyclopropane limiting form, for the fluoride system. This result, contrary to the expectation based on the halide electronegativity and the computed charge on the metal atom, is, nevertheless, in agreement with the computed longer C═C distance in $\mathbf{1}^F$ and $\mathbf{2}^F$, decreasing on going down the halogen series. Hence, the fluoride coligands, even though pulling more electron density away from the metal atom via the σ-bonding framework, provide more electron density in return via the π mechanism. In other words, the F^- ligands are worse σ-donors, but better π-donors, than the other halides and allow the metal to provide more back-bonding to the ethylene ligand. Given the orientation of the ethylene ligand perpendicular to the

Table 1. Selected Natural Charge and Bond Distances in Systems $\mathbf{1}^X$, $\mathbf{2}^X$, $\mathbf{3}^X$, and $\mathbf{TS2}^X$

	q_{Pt} (NBO)	$q_{X\ trans}$ (NBO)	$q_{X\ cis}$[a] (NBO)	q_C (NBO)	Pt−C (*d*/Å)	C═C (*d*/Å)	
$\mathbf{1}^F$	1.022	−0.650	−0.640	−0.523	2.089	1.415	
$\mathbf{1}^{Cl}$	0.269	−0.445	−0.430	−0.482	2.131	1.410	
$\mathbf{1}^{Br}$	0.070	−0.382	−0.367	−0.480	2.145	1.408	
$\mathbf{1}^I$	−0.251	−0.274	−0.266	−0.478	2.166	1.405	
	q_{Pt} (NBO)	q_N (NBO)	$q_{X\ cis}$[a] (NBO)	q_C (NBO)	Pt−C (*d*/Å)	C═C (*d*/Å)	Pt−N (*d*/Å)
$\mathbf{2}^F$	0.875	−0.842	−0.624	−0.467	2.136	1.400	2.123
$\mathbf{2}^{Cl}$	0.350	−0.821	−0.406	−0.446	2.158	1.398	2.133
$\mathbf{2}^{Br}$	0.216	−0.821	−0.338	−0.446	2.164	1.398	2.137
$\mathbf{2}^I$	0.002	−0.822	−0.230	−0.444	2.173	1.398	2.151
		q_{Pt} (NBO)	q_N[b] (NBO)		$q_{X\ cis}$[a] (NBO)		Pt−N (*d*/Å)
$\mathbf{3}^F$		0.754	−0.815		−0.658		2.063
$\mathbf{3}^{Cl}$		0.312	−0.794		−0.468		2.075
$\mathbf{3}^{Br}$		0.191	−0.795		−0.406		2.081
$\mathbf{3}^I$		−0.006	−0.796		−0.305		2.092
	q_{Pt} (NBO)	$q_{X\ trans}$ (NBO)	q_H (NBO)	q_C (NBO)	Pt−C (*d*/Å)	C═C (*d*/Å)	Pt−H (*d*/Å)	C−H (*d*/Å)
TS2F	0.873	−0.629	0.191	−0.661	2.195		1.584	1.435
$\mathbf{TS2}^{Cl}$	0.132	−0.424	0.212	−0.587	2.203		1.571	1.548
$\mathbf{TS2}^{Br}$	−0.065	−0.364	0.209	−0.577	2.212		1.571	1.567
$\mathbf{TS2}^I$	−0.378	−0.261	0.204	−0.569	2.226		1.573	1.580

[a]Average value for the *cis*-X atoms in systems $\mathbf{1}^X$, $\mathbf{2}^X$, and $\mathbf{3}^X$. [b]Average value for the two N atoms in system $\mathbf{3}^X$.

dx.doi.org/10.1021/om2009149 | *Organometallics* 2012, 31, 294−305

coordination plane, this interaction occurs via the metal d_{xz} orbital, where x is the axis along the C_2H_4(center)-Pt-X_{trans} vector. A qualitative orbital interaction diagram of the π interaction for the $\mathbf{1}^{X}$ system is shown in Figure 3.

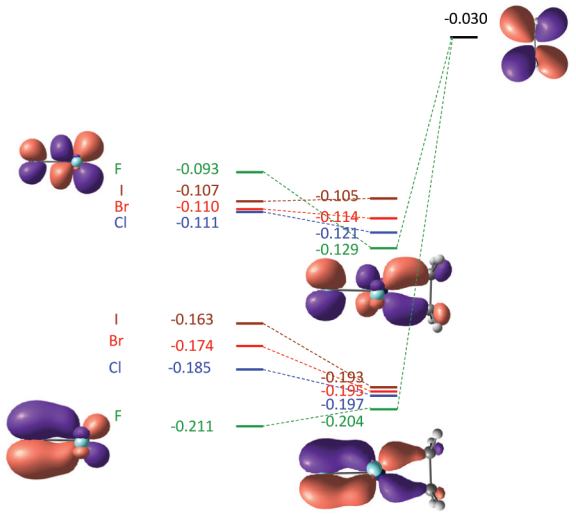

Figure 3. Orbital interaction responsible for the Pt−C_2H_4 back-bonding in complexes $\mathbf{1}^{X}$ (see text). The orbital energies are in electronvolts. Representative contour diagrams are only shown for the fluoride system (for the complete set of MOs, see the Supporting Information).

To a first approximation, only the *trans*-X atom participates in the interaction with its p_z orbital. The $[PtX_3]^-$ fragment on the left of the interaction diagram participates with two filled orbitals, resulting from the in-phase and out-of-phase combination of the *trans*-X p_z orbitals and the Pt d_{xz} orbital, which results in no net X−Pt π-bonding. The greater electronegativity in the order F > Cl > Br > I is reflected in an energy decrease along the same sequence, with the exception of the F system, for which the out-of-phase combination is raised above those of the other halogen systems, whereas the in-phase combination is unusually stabilized relative to those of the other three systems. This is already a clear indication of the stronger π interaction occurring for the F system. Now, both orbitals have the correct symmetry to interact and be stabilized by the ethylene CC π^* combination (on the right of the interaction diagram), a phenomenon widely known as push−pull interaction.[44] The net result is transmission of electron density from the halogen p_z orbital to the ethylene π^* orbital with the consequent increase of C−C distance and natural charge of the ethylene C atoms. As shown in Figure 3, the establishment of these interactions clearly leads to a stronger stabilization for the out-of-phase combination in the case of the F system. The donor orbital (the out-of-phase F_{trans}−Pt xz combination at −0.093 eV) is much more Pt(d_{xz}) in character and higher in energy relative to the other halogen systems, thus resulting in a stronger transfer of electron density from the F atom p_z orbital to the CC π^* combination. This effect is partly counterbalanced by that of the in-phase combination, which grows in importance on going from F to I because the in-phase combination becomes more and more Pt(d_{xz})-like as X becomes heavier (hence, stronger back-bonding to ethylene), whereas the out-of-phase combination becomes more and more X(p_z)-like (hence, weaker back-bonding to ethylene). The overall balance is much in favor of stronger (X_{trans}Pt)−(C_2H_4) back-bonding as the halogen gets lighter, with the biggest gap between Cl and F.

For systems $\mathbf{2}^{X}$, the ligand trans to ethylene (aniline) is common to all complexes and the cis halogen atoms give rise to a weaker π effect. The resulting q_C and CC distance variations are smaller, although still in the direction expected for a more important contribution of the π-bonding mechanism. Counter-intuitively, the calculated natural charge on the aniline N atoms in systems $\mathbf{2}^{X}$ and $\mathbf{3}^{X}$ is also more negative for the complexes containing more electronegative halogen atoms, the biggest gap being once again between the F and Cl systems, although this variation is less pronounced relative to that on the ethylene C atoms in system $\mathbf{1}^{X}$, which is paralleled by shorter Pt−N distances. In this case, it does not seem possible to attribute the observed change to a π-bonding interaction, since aniline is not a π acid. A σ effect through the hardness/softness concept[45−47] could be held responsible for this trend, the harder F atom rendering the Pt−N bond more ionic/less covalent. The Pt−N natural charge difference gets smaller on going to the heavier halide systems, which is accompanied by a lengthening of the Pt−N bond.

Now the trend observed for the energy change on going from $\mathbf{1}^{X}$ to $\mathbf{2}^{X}$ can be rationalized. Indeed, the replacement of a π-donating X^- ligand with the π-neutral $PhNH_2$ decreases the effect of the special π-stabilizing effect of the F^- ion and flattens the relative stability between the species, probably because of a more balanced compensation between σ and π effects. On going further from $\mathbf{2}^{X}$ to $\mathbf{3}^{X}$, the ethylene ligand is replaced by a second aniline ligand and the residual small π synergism that was present in $\mathbf{2}^{X}$ is no longer possible. Hence, the fluoride system is destabilized by a greater amount than the other three systems, for which the exchange is essentially thermoneutral.

The transition states $\mathbf{TS2}^{X}$ were also optimized; see Figure 2. The free energy relative to the resting state, $G(\mathbf{TS2}^{X}) - G(\mathbf{1}^{X})$, is a direct measure of $\Delta G^{\ddagger}_{cycle}$, related to the turnover frequency under standard conditions.[41,42] This value varies in a non-monotonous way, increasing from F to Cl, then decreasing from Cl to Br, and finally increasing again from Br to I. Note that, for the three systems that were investigated experimentally (Cl, Br, I), the computational result is in qualitative agreement with the experimental results shown in Table 2.[28] However, we must be cautious to make a direct comparison, because only TON values were reported for the different halide systems. The $\Delta G^{\ddagger}_{cycle}$ parameter can be related by the Eyring expression to the turnover frequency (TOF), which was not measured, and not to the TON. Given that the TON values were obtained under the same conditions and after the same period (10 h), they should be proportional to the TOF, assuming no catalyst degradation. However, we know that the catalyst is irreversibly degraded during the catalytic runs to metallic Pt, which is

Table 2. Hydroamination of Ethylene by Aniline Catalyzed by [$PtBr_2$]/$n$$Bu_4$PX[a]

$n$$Bu_4$PX	total TON 10 equiv $n$$Bu_4$PX	total TON 65 equiv $n$$Bu_4$PX	total TON 150 equiv $n$$Bu_4$PX
$n$$Bu_4$PF	not studied	not studied	not studied
$n$$Bu_4$PCl	50	105	80
$n$$Bu_4$PBr	150	130	88
$n$$Bu_4$PI	135	100	5

[a]Data from ref 28. Conditions: $PtBr_2$, 0.13 mmol; $PhNH_2$, 45 mmol; $p(C_2H_4)$ = 25 bar at 298 K (ca. 100 mmol); 150 °C; 10 h.

dx.doi.org/10.1021/om2009149 | *Organometallics* 2012, 31, 294−305

inactive for the hydroamination process.[26,48] Hence, the greater TON observed for the Br system might be simply the result of slower catalyst degradation. Note also that the maximum activity for each halide system (in terms of TON, Table 2) was observed for a different excess amount of the activating salt (65 equiv for the chloride, 10 equiv for the bromide and iodide). The computed values relate, on the other hand, to the standard conditions (1 M concentrations for all species).

One relevant and interesting result of the calculations is that the lowest $\Delta G^{\ddagger}_{cycle}$ is, in fact, calculated for the F system, which has not yet been experimentally investigated ($^{n}Bu_4PF$ is less readily available), suggesting that the PtX_2/X^- catalyst may have a greater catalytic efficiency when X = F. Note that a positive effect of fluoride was experimentally demonstrated for the iridium-catalyzed hydroamination of norbornene by aniline.[49] For this reason, as well as for removing the doubt about catalyst degradation, new experimental measurements were carried out for this catalytic process with monitoring of the kinetic profile, in the presence of an equivalent amount of all halides, I^-, Br^-, Cl^-, and F^- (see next section).

For the sake of completion, we have also carried out a natural charge analysis on the TOF-determining transition state **TS2**^{X}; see Table 1. The same trends observed above for the halide and metal charge in **1**^{X} are also observed in **TS2**^{X}. The negative charge on the Pt-bonded C atom decreases systematically on moving from F to I, indicating that the alkyl group is still sufficiently bonded to the metal to feel the competitive inductive effect of the halide ligands. The H atom moves from Pt to C as a proton (positive charge, approximately halogen-independent) and the transition state has an "earlier" character (the C−H distance becomes longer, whereas the Pt−C and Pt−H remain approximately unchanged) as the X atoms become heavier.

b. New Catalytic Studies. A comparison of the four halide salts is legitimate if all conditions are perfectly identical except for the nature of the halide ion. Namely, the cation should be the same. The effect of chloride, bromide, and iodide was studied using the *n*-butylphosphonium salts, all being commercially available (Cl, Br) or easily synthesized (I). In the case of the fluoride salt, we did not find a convenient access to nBu_4PF, and so we wondered whether the nature of the cation is really important. A readily available fluoride salt is $nBu_4NF{\cdot}3H_2O$. To see whether using this salt for comparison could be justified, we have run a few additional catalytic experiments with the following bromide salts as catalyst additives: nBu_4PBr (classical conditions),[26] *n*-Bu_4NBr, and *n*-$Bu_4NBr{\cdot}3H_2O$. These three salts give essentially equivalent results (see Table 3, runs 1−3), showing that the process is not significantly affected by the cation nature and by the presence of water. Incidentally, we had already established that similar catalytic activities and an identical selectivity could be achieved by activation with aqueous NaBr.[48]

Table 3. Hydroamination of Ethylene by Aniline Catalyzed by $[PtBr_2]/nBu_4PX$[a]

run	additive	TON PhNHEt	TON $PhNEt_2$	TON quinaldine
1	nBu_4PBr	97	1	10
2	nBu_4NBr	119	2	8
3	$nBu_4NBr{\cdot}3H_2O$	104	2	7
4	nBu_4NF	6	0	2
5	$nBu_4NF{\cdot}3H_2O$	2	0	2

[a]Conditions: $PtBr_2$, 0.13 mmol; salt additive, 1.3 mmol; $PhNH_2$, 45 mmol; $p(C_2H_4)$ = 25 bar at 298 K (ca. 100 mmol); 150°C; 10 h.

Hence, we could proceed to catalytic tests using *n*-$Bu_4NF{\cdot}3H_2O$. The experiment, carried out under the classical conditions, gave disappointing results, which did not significantly change after drying the salt (Table 3, runs 4 and 5). This result could remain consistent with the high activity suggested by the calculated $\Delta G^{\ddagger}_{cycle}$ only if the fluoride system is affected by a more severe catalyst decomposition process or if fluoride exerts another function in addition to coordinating the Pt center. The next series of experiments aimed at obtaining the relative initial activities through a determination of the kinetic profile. These experiments were carried out under nearly identical conditions as those of the previous runs (e.g., those shown in Tables 2 and 3), with double amounts of all reagents in order to have enough material in the autoclave for multiple sampling. The only exception was C_2H_4, which was maintained at the same pressure. However, its available amount relative to aniline is still sufficient to satisfy the reaction stoichiometry. The results are reported in Figure 4.

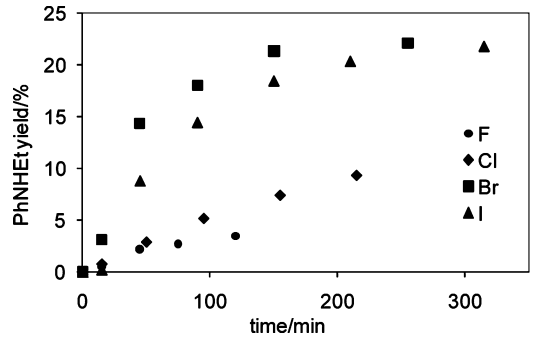

Figure 4. Kinetic profiles of the hydroamination of C_2H_4 by aniline, catalyzed by $PtBr_2/nBu_4PX$ (X = Cl, Br, I) or $PtBr_2/nBu_4NF{\cdot}3H_2O$. Conditions: $PtBr_2$, 0.26 mmol; salt additive, 2.6 mmol; $PhNH_2$, 90 mmol; $p(C_2H_4)$ = 25 bar at 298 K (ca. 100 mmol); 150 °C.

The analysis of these data leads to several considerations. The first one is the limited catalyst lifetime in each case. At the end of the catalytic run, massive amounts of both aniline and ethylene are still present in the autoclave, but the catalytic activity is reduced essentially to zero after just 6 h, at least for the most-active Br and I systems. Metallic platinum, as previously reported,[26,48] was found in the product mixture. The second consideration is that, limited to the heavier halogens, Cl, Br and I, the initial activity is in qualitative agreement with the original report by Brunet et al., which was based on the TON after 10 h (activity in the order Br > I ≫ Cl). Thus, even though the system is heavily affected by catalyst decomposition, a qualitative direct relationship between initial TOF and TON exists.[26] The third observation is that the fluoride system, contrary to the computational prediction, is the least-active system. Its initial slope is not any greater than that of the chloride system, and furthermore, it seems to deactivate faster, the percent yield no longer increasing significantly after 45 min, whereas the other halogen systems continue to produce the *N*-ethylaniline product. The data, therefore, suggest that fluoride not only leads to a faster catalyst decomposition but also exerts another function in addition to coordinating the Pt center.

To rationalize this result, we consider that one important difference between F^- and the heavier halides is its basicity. We

dx.doi.org/10.1021/om2009149 | *Organometallics* 2012, 31, 294−305

have recently shown that the use of a basic amine, notably $NHEt_2$, leads to a more favorable nucleophilic addition to the coordinated ethylene, with generation of equilibrium amounts of the zwitterionic intermediate that could be fully characterized (contrary to aniline for which this intermediate is unobservable), but the excess amine leads to a deprotonation equilibrium with the aminoalkyl species, incapable of proceeding along the hydroamination cycle, and leads to the system decomposition with generation of metallic platinum, as also pointed out by other previous related studies,[50−52] by a pathway that is not yet understood.[53] Metallic platinum was proven catalytically inactive for the hydroamination process. Hence, it may be proposed that the F^- ion leads to a faster catalyst deactivation through its stronger basic character. The $NHEt_2$-induced zwitterion deprotonation was also analyzed by DFT calculations.[53] We did not consider it useful to carry out additional calculations in the presence of an extra halide ion. On the other hand, we checked the hypothesis of a base-related deactivation through additional experimental studies.

As we have recently reported and already mentioned above, the $[PtBr_3(C_2H_4)]^-$ system is also catalytically active when generated through the use of aqueous NaBr (the K_2PtCl_4 precatalyst was more conveniently used in this case).[48] The same conditions have now been used in the presence of added bases, namely, $NHEt_2$, NEt_3, and 1,8-diazabicyclo[5.4.0]undec-7-ene (DBU). As shown by the results in Table 4, the addition of the base completely suppresses the catalytic activity. This is also and especially true for bases, such as NEt_3 and DBU, that combine high basicity with poor nucleophilicity. In the absence of any external base (fluoride or a stronger amine), the catalyst is still deactivated, though more slowly, by the action of aniline itself. Fluoride is a weaker base (pK_a = 3.18) than aniline (pK_a = 4.62) in water, but its basicity is enhanced by up to 3 orders of magnitude in lower polarity solvents.[54] On the basis of these results, it is also possible to rationalize the previously highlighted positive effect of a catalytic amount of a strong acid as an additive to the $PtBr_2/Br^-$ system.[26] The strong acid (CF_3COOH in the reported study) in the $PhNH_2$-rich medium generates an equivalent amount of $PhNH_3^+$, which buffers the action of free aniline in the deprotonation of the zwitterionic intermediate and, therefore, retards the deactivation process.

Table 4. $[K_2PtCl_4]$/NaBr-Catalyzed Hydroamination of Ethylene by Aniline in the Presence of Bases[a]

run	base	TON PhNHEt	TON $PhNEt_2$	TON quinaldine
1		85	1	8
2	$NHEt_{2\ his}$	1	0	~0.5
3	NEt_3	0.5	0	0
4	DBU	0.4	0	0

[a]Conditions: K_2PtCl_4, 0.13 mmol; NaBr, 19.5 mmol; $PhNH_2$, 45 mmol; $p(C_2H_4)$ = 25 bar at 298 K (ca. 100 mmol); H_2O, 15 mL; base, 1.3 mmol; 150 °C; 10 h.

c. Additional Experimental Mechanistic Studies. To learn more about how the basicity affects the catalyst stability, a few additional experiments have been carried out. First, two control experiments probed the catalyst stability in a mixture where one of the two reaction components (aniline and ethylene) is left out. The experiments were run under the same conditions of time (10 h) and temperature (150 °C) as the catalytic runs. A first experiment involved warming up $PtBr_2$ in pure aniline in the presence of nBu_4PBr without ethylene. This run could be carried out in regular glassware since aniline boils at 184 °C. The result is dissolution of $PtBr_2$ to yield a Bordeaux-red solution, from which a powdery brown precipitate deposited upon cooling. This product may correspond to $(nBu_4P)[PtBr_3(PhNH_2)]$, previously obtained by anion exchange from K_2PtCl_4 in the presence of aniline.[40] For the purpose of this test, however, the exact nature of this product is irrelevant and characterization was not pursued. The important point is that the solution was filtered and the solid washed out completely with a variety of solvents (dichloromethane, acetone, ethanol...), leaving on the filter only traces of insoluble residue that could possibly correspond to metallic platinum. A second experiment was carried out in the presence of ethylene and in the absence of aniline. Because aniline is also the catalysis solvent in the classical procedure,[26] the test was carried out by replacing aniline with toluene. The result of this experiment is the complete dissolution of $PtBr_2$, yielding a clear red solution and notably containing no visible amounts of black Pt^0. Precipitation by addition of diethyl ether yielded an orange crystalline product, the ^1H NMR of which confirmed that this is the known $nBu_4P[PtBr_3(C_2H_4)]$ by comparison with an authentic sample.[40]

These two tests clearly indicate the thermal stability of Pt^{II} and resistance to reduction in the coordination environment provided by bromide anions in combination with either ethylene or aniline. The reduction must, therefore, be a consequence of the combined action of both reagents. A working hypothesis is that the base acts on intermediate $\mathbf{4^{Br}}$ (Table 1), obtained after nucleophilic addition of aniline to the coordinated ethylene. A logical possibility is deprotonation of the ammonium function, but other possibilities may also be considered, such as reversible β-H elimination, followed by deprotonation of the resulting Pt(II) hydride species, whereas the deprotonation of the Pt(IV) hydride complex subsequently formed along the hydroamination cycle ($\mathbf{5^{Br}}$) would not lead to the generation of metallic platinum. These hypotheses for the catalyst decomposition will be further probed from the experimental and computational viewpoints in forthcoming investigations and published in due course.

d. Effect of the $ArNH_2$ Basicity. As mentioned in the Introduction, the catalytic activity for the Brunet system, as measured by the TON obtained under the same conditions for a variety of substituted anilines $ArNH_2$, is inversely proportional to the amine basicity: 22 for 4-$MeOC_6H_4$ (pK_a = 5.34), 55 for C_6H_5 (pK_a = 5.08), 90 for 4-ClC_6H_4 (pK_a = 4.15), and 110 for 2-ClC_6H_4 (pK_a = 2.65).[26] In light of the discussion offered in the preceding sections, this trend would simply result from a different rate of catalyst deactivation, faster for more basic anilines. We were interested, however, to see whether the electronic structure of the aniline would also affect the intrinsic activity in terms of the $\Delta G^{\ddagger}_{cycle}$. Therefore, we have run additional calculations with two modified anilines, 4-$MeOC_6H_4NH_2$ and 4-$ClC_6H_4NH_2$, restricted to the bromide system. These calculations included the transition states $\mathbf{TS2^{BrOMe}}$ and $\mathbf{TS2^{BrCl}}$, and the corresponding complexes *trans*-$[PtBr_2(C_2H_4)(ArNH_2)]$ ($\mathbf{2^{BrOMe}}$ with Ar = 4-$MeOC_6H_4$ and $\mathbf{2^{BrCl}}$ with Ar = 4-ClC_6H_4). We did not calculate the corresponding *trans*-$[PtBr_2(ArNH_2)_2]$ derivatives (**3**). The results are compared with those of the previously calculated $\mathbf{2^{Br}}$ and $\mathbf{TS2^{Br}}$ systems in Figure 5. Once again, species $\mathbf{1^{Br}}$ is, in every case, the most stable one, both at room temperature and at the temperature used for catalysts (resting state). The calculations yield $\Delta G^{\ddagger}_{cycle}$ values growing with the aniline

dx.doi.org/10.1021/om2009149 | *Organometallics* 2012, 31, 294−305

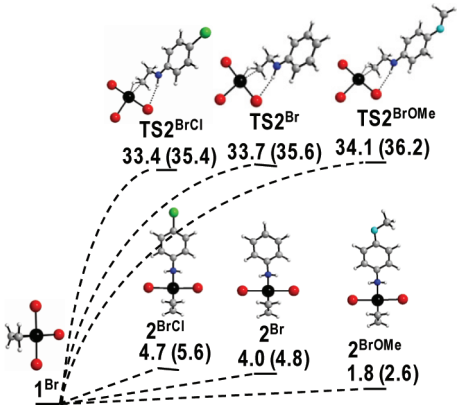

Figure 5. Relative Gibbs free energy of the *trans*-$PtBr_2(C_2H_4)(ArNH_2)$ (Ar = 4-C_6H_4OMe, $\mathbf{2}^{BrOMe}$; C_6H_5, $\mathbf{2}^{Br}$; 4-C_6H_4Cl, $\mathbf{2}^{BrCl}$) and the corresponding TOF-determining transition states ($\mathbf{TS2}^{BrOMe}$, $\mathbf{TS2}^{Br}$, $\mathbf{TS2}^{BrCl}$). Values are ΔG^{CPCM} (aniline) relative to $[PtBr_3(C_2H_4)]^-$ ($\mathbf{1}^{Br}$) in kcal mol^{-1} at 298.15 K (and at 423.15 K in parentheses).

basicity, which agrees with the experimental observed greater activity for the addition of less basic anilines. Hence, the observed activity trend may result from an intrinsic aniline basicity effect on $\Delta G^{\ddagger}_{cycle}$, or from a lower propensity of the less basic aniline to deactivate the catalyst, or from a combination of these two effects.

The natural charge analysis of transition states $\mathbf{TS2}^{BrCl}$ and $\mathbf{TS2}^{BrOMe}$ (Table 5) do not reveal dramatic changes relative to

Table 5. Selected Natural Charge and Bond Distances in Systems $\mathbf{TS2}^{BrCl}$ and $\mathbf{TS}^{BrOMe}$

	$\mathbf{TS2}^{BrCl}$	$\mathbf{TS2}^{BrOMe}$
q_{Pt} (NBO)	−0.067	−0.066
$q_{trans\text{-}Br}$ (NBO)	−0.359	−0.365
q_H (NBO)	0.209	0.208
q_C (NBO)	−0.579	−0.574
C−H, *d* (Å)	1.566	1.570
Pt−H, *d* (Å)	1.572	1.570
Pt−C, *d* (Å)	2.211	2.213

the corresponding parameters of $\mathbf{TS2}^{Br}$ analyzed above in Table 1. In particular, the charge on the Pt center remains approximately unaffected. The most notable change is the less negatively charged Br^- for the *p*-chloroaniline derivative relative to the other two derivatives. As the aniline becomes more basic, the Pt-bonded C atom engaged in the reductive elimination becomes less negatively charged, while the geometry of the PtHC moiety experiences very minor variations.

e. Hydroamination of 1-Hexene. As highlighted in a recent review,[29] many active catalysts for ethylene hydroamination fail when applied to higher olefins. Previous work on the PtX_2/X^- catalytic system, however, has shown a relatively high activity also for the hydroamination of 1-hexene, even though slightly lower than for the ethylene hydroamination (under the same conditions, namely, 10 h at 150 °C with 0.3% catalyst and 65 equiv of nBu$_4$PBr per Pt; 1-hexene yields 57 turnovers[27] vs 131 for ethylene[26]). This activity difference is not likely due to a difference in catalyst deactivation rate, since the deactivation process is now known to be related to the action of an external base (which ethylene and 1-hexene are not) on the zwitterionic intermediate and the above comparative productivities were obtained under strictly identical conditions except for the olefin. Therefore, the different activity is probably related to a greater activation barrier ($\Delta G^{\ddagger}_{cycle}$) when going from ethylene to the higher olefin. It was also shown that the Markovnikov product is highly favored (95:5),[27] and the best results (highest TON) were obtained, in this case, in the presence of the iodide salt.[28]

Our aim is to use computational chemistry to compare the aniline addition to 1-hexene and ethylene with the PtX_2/X^- catalytic system. The calculation of the thermodynamic gain of the reaction (see Table 6) shows that the hydroamination of 1-hexene is slightly less favorable than that of ethylene and that the Markovnikov product is slightly favored on the *H* and *G* scales in the gas phase, although the preference reverses in favor of the anti-Markovnikov product when considering the solvent effect of aniline by the C-PCM.

1. Markovnikov vs anti-Markovnikov Regioselectivity. Calculations to address this issue were carried out only for the bromide system, since the 95:5 regioselectivity is essentially independent of the nature of the halide.[28] Following our previous work on the catalytic cycle for ethylene (see the Introduction), at least five 1-hexene complexes are potentially susceptible to aniline nucleophilic addition, namely, $[PtBr_3(1\text{-hexene})]^-$, *cis*- and *trans*-$[PtBr_2(1\text{-hexene})(PhNH_2)]$, and *cis*- and *trans*-$[PtBr_2(1\text{-hexene})_2]$.

The calculations started with complexes $[PtBr_3(1\text{-hexene})]^-$ ($\mathbf{1}^{Br}_{hex}$) and *trans*-$[PtBr_2(1\text{-hexene})(PhNH_2)]$ ($\mathbf{2}^{Br}_{hex}$), which represent the 1-hexene analogues of the resting state and the next most stable olefin-containing complex for the ethylene system. Relative to $[PtBr_4]^{2-}$, 1-hexene coordination provides a smaller stabilization than ethylene by 4.7 kcal mol^{-1} for $\mathbf{1}^{Br}_{hex}$ (−9.9 kcal mol^{-1} relative to −14.6 kcal mol^{-1} for $\mathbf{1}^{Br}$) and by 3.3 kcal mol^{-1} for $\mathbf{2}^{Br}_{hex}$ (−7.4 kcal mol^{-1} relative to −10.7 kcal mol^{-1} for $\mathbf{2}^{Br}$). Calculations on the 1-hexene analogues of the other, higher-energy systems were not carried out. We recall, however, that compound *trans*-$[PtBr_2(PhNH_2)_2]$, $\mathbf{3}^{Br}$, is placed at −11.0 kcal mol^{-1} relative to $[PtBr_4]^{2-}$ on the G^{CPCM} (aniline) scale at 298 K.[39] Hence, while $\mathbf{1}^{Br}$ is the resting state for the ethylene system, the analogous complex $\mathbf{1}^{Br}_{hex}$ is slightly less stabilized than $\mathbf{3}^{Br}$. Calculations, including the thermochemical corrections at 423.15 K, however, place compound $\mathbf{1}^{Br}_{hex}$ 0.25 kcal/mol lower in relative

Table 6. Thermodynamic Data for the Hydroamination of Ethylene and 1-Hexene by Aniline in the Gas Phase and in Aniline as Solvent[a]

reaction	$\Delta S°$ (e.u.)	$\Delta H°$ (kcal/mol)	$\Delta G°$ (kcal/mol)	ΔG^{CPCM} (kcal/mol)
$C_2H_4 + PhNH_2 \rightarrow PhNHEt$[b]	−37.4 (−37.4)	−17.2 (−17.2)	−6.0 (−1.4)	−8.0 (−6.3)
$C_4H_9CH{=}CH_2 + PhNH_2 \rightarrow C_4H_9CH(NHPh)CH_3$	−41.9 (−41.6)	−13.4 (−13.3)	−0.9 (4.4)	−1.1 (1.0)
$C_4H_9CH{=}CH_2 + PhNH_2 \rightarrow C_4H_9CH_2CH_2NHPh$	−41.8 (−41.9)	−12.1 (−12.1)	0.4 (5.6)	−1.5 (0.4)

[a]The data refer to 298.15 K, with those at 423.15 K in parentheses. [b]Data from ref 39.

dx.doi.org/10.1021/om2009149 | *Organometallics* 2012, 31, 294−305

G^{CPCM}(aniline) than $\mathbf{3}^{Br}$. Therefore, the resting state of the catalytic cycle for the 1-hexene hydroamination is either $\mathbf{1}^{Br}_{hex}$ or the off-loop species $\mathbf{3}^{Br}$ depending on the temperature. It should also be mentioned that, under conditions similar, but not totally identical, to those of the hydroamination catalysis, $[PtBr_4]^{2-}$ was recently shown to afford $[PtBr_5]^{3-}$ in the presence of a large excess of a bromide salt and that the latter species does not react with 1-hexene.[55]

Because it was shown that the only productive zwitterionic intermediate for the ethylene system is that derived from the anionic tribromo complex (Figure 1), we have only examined the aniline addition to $\mathbf{1}^{Br}_{hex}$, considering, however, both the CH_2 and the CHBu groups to yield zwitterionic complexes of Markovnikov ($\mathbf{4}^{Br}_{hex}\mathbf{M}$) and anti-Markovnikov ($\mathbf{4}^{Br}_{hex}\mathbf{A}$) types. Several local minima were found for each addition product, the most stable ones being outlined in Figure 6. Both types of

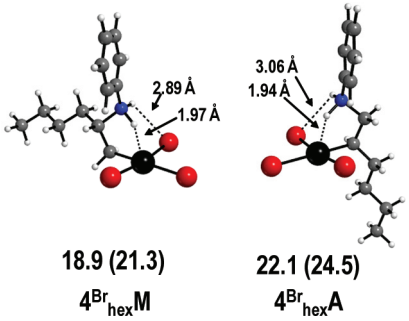

Figure 6. Geometries and relative Gibbs free energies of the most stable products of $PhNH_2$ addition to the CHBr ($\mathbf{4}^{Br}_{hex}\mathbf{M}$) and CH_2 ($\mathbf{4}^{Br}_{hex}\mathbf{A}$) groups of the coordinated 1-hexene in $[PtBr_3(1\text{-hexene})]^-$ ($\mathbf{1}^{Br}_{hex}$). Values are ΔG^{CPCM} (aniline) in kcal mol^{-1} relative to $\mathbf{1}^{Br}_{hex}$ at 298.15 K (and at 423.15 K in parentheses).

$PhNH_2$ additions are slightly less favorable thermodynamically relative to the addition to ethylene (18.2 kcal mol^{-1}; see Figure 1), with $\mathbf{4}^{Br}_{hex}\mathbf{M}$ being less destabilized than $\mathbf{4}^{Br}_{hex}\mathbf{A}$. The geometries of the two products are closely related to that of the ethylene analogue $\mathbf{4}^{Br}$, with a short N−H···Pt hydrogen bond, predisposed for proton transfer to the platinum center, and a less tight hydrogen bond connecting a second N−H bond with one of the bromine atoms.

We have also analyzed the activation barriers for the aniline nucleophilic addition ($\mathbf{TS1}^{Br}_{hex}$). The shape of the LUMO of complex $\mathbf{1}^{Br}_{hex}$ (Figure 7) clearly suggests that the C2 atom

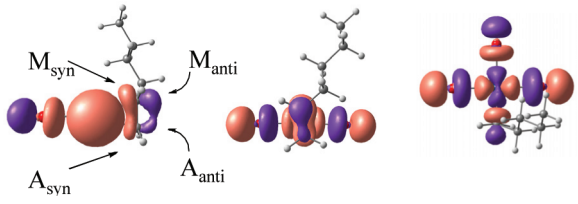

Figure 7. Three mutually orthogonal views of the LUMO (E = 0.0424 hartree) of complex $\mathbf{1}^{Br}_{hex}$, with indication of all possible pathways for nucleophilic aniline addition.

should be more easily attacked by the aniline nucleophile. The NBO analysis yields the charges of −0.48 for C1 and −0.24 for C2. Therefore, charge control also favors attack at the C2 atom. The figure also indicates the four possible pathways for nucleophilic addition: two *anti* attacks (M_{anti} and A_{anti}) and two *syn* attacks (M_{syn} and A_{syn}). For each type of attack, there are actually two different pathways, depending on the direction in which the attached C atom will twist. Only the lower-energy transition state for each type of attack is shown in Figure 8. The

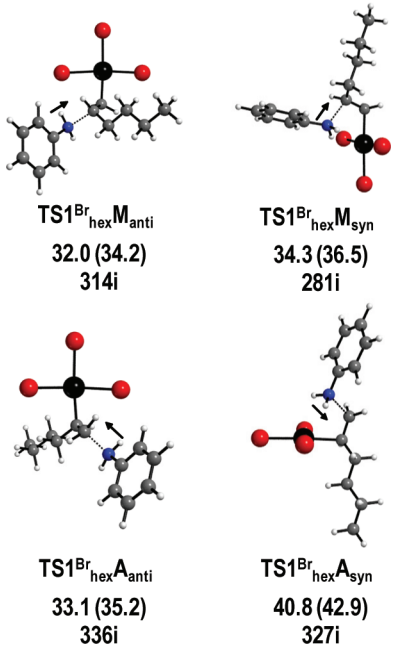

Figure 8. Views of the lowest-energy transition states for the four types of nucleophilic addition of $PhNH_2$ to coordinated 1-hexene in $\mathbf{1}^{Br}_{hex}$. Values of ΔG^{CPCM} (aniline) in kcal mol^{-1} relative to $[PtBr_3(1\text{-hexene})]^-$ ($\mathbf{1}^{Br}_{hex}$) at 298.15 K (and at 423.15 K in parentheses) and of the calculated imaginary frequency in cm^{-1} are also shown.

calculations indicate that for each C atom, the anti attack is favored (the same result was previously found[39] for the $PhNH_2$ to ethylene in $\mathbf{1}^{Br}$) and that the Markovnikov attack is kinetically preferred by ca. 1 kcal mol^{-1}. Hence, the lowest transition state is $\mathbf{TS1}^{Br}_{hex}\mathbf{M}_{anti}$, leading to the Markovnikov zwitterionic complex $\mathbf{4}^{Br}_{hex}\mathbf{M}$. However, the difference between the two barriers is irrelevant for the regioselectivity of the catalysis reaction, because the turnover rate for both Markovnikov and anti-Markovnikov products is determined by the final reductive elimination step (vide infra).

The next step in the mechanism is proton transfer from the ammonium function of the zwitterionic intermediate to the Pt atom, yielding the 5-coordinate $\mathbf{5}^{Br}_{hex}\mathbf{M}$ and $\mathbf{5}^{Br}_{hex}\mathbf{A}$ complexes shown in Figure 9. Like for the zwitterionic precursors $\mathbf{4}^{Br}_{hex}\mathbf{M}$ and $\mathbf{4}^{Br}_{hex}\mathbf{A}$, complexes $\mathbf{5}^{Br}_{hex}$ exhibit a stabilizing intramolecular N−H···Br interaction and the Markovnikov product is slightly more stable.

Starting from these complexes, the product is generated by C−H reductive elimination through the TOF-determining transition state $\mathbf{TS2}^{Br}_{hex}$, leading to a σ-complex $\mathbf{6}^{Br}_{hex}$, where the newly formed C−H bond remains placed in correspondence to one of the coordination sites of the square-planar Pt^{II} center. All geometries are depicted in Figure 10. For the anti-Markovnikov product $\mathbf{6}^{Br}_{hex}\mathbf{A}$, no significant interaction with the C atom is observed but the H atom remains in close contact with the Pt center (the Pt···H−C angle is more open). Another peculiarity, revealed by IRC calculations from the optimized transition states, is that another local minimum exists for the Markovnikov pathway between the hydride complex $\mathbf{5}^{Br}_{hex}\mathbf{M}$

dx.doi.org/10.1021/om2009149 | Organometallics 2012, 31, 294−305

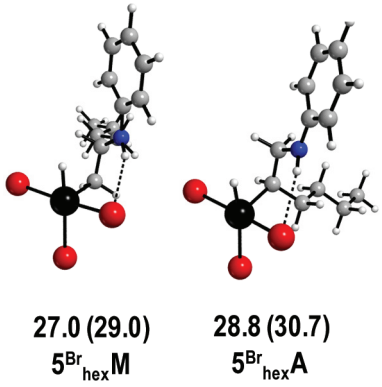

Figure 9. Geometries and relative Gibbs free energies of the Pt^{IV} hydride intermediates $\mathbf{5}^{Br}_{hex}\mathbf{M}$ and $\mathbf{5}^{Br}_{hex}\mathbf{A}$. Values are ΔG^{CPCM} (aniline) in kcal mol^{-1} relative to $[PtBr_3(1\text{-hexene})]^-$ ($\mathbf{1}^{Br}_{hex}$) at 298.15 K (and at 423.15 K in parentheses).

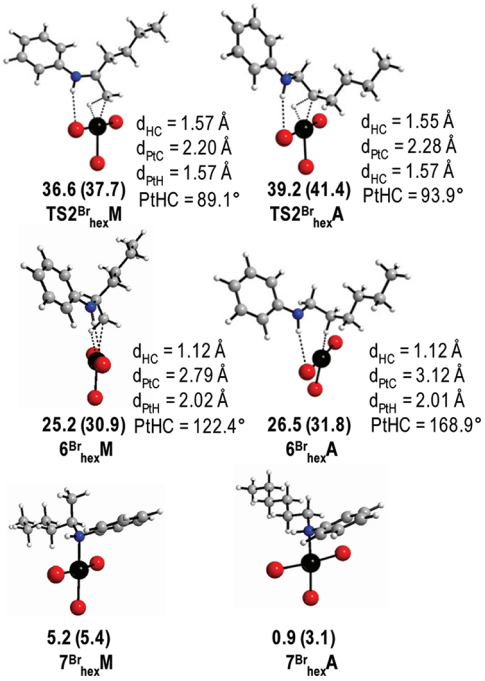

Figure 10. Geometries and relative Gibbs free energies of the transition states and products, $\mathbf{TS2}^{Br}_{hex}$ and $\mathbf{6}^{Br}_{hex}$, of the C–H reductive elimination from the hydride complexes $\mathbf{5}^{Br}_{hex}$, as well as of the products of rearrangement of the *N*-1- or *N*-2-hexylaniline, $\mathbf{7}^{Br}_{hex}$. Values are ΔG^{CPCM} (aniline) in kcal mol^{-1} relative to $[PtBr_3(1\text{-hexene})]^-$ ($\mathbf{1}^{Br}_{hex}$) at 298.15 K (and at 423.15 K in parentheses).

and the transition state, characterized by a trigonal-bipyramidal geometry with equatorial Br, H, and $CH_2CH(Bu)NHPh$ ligands, at higher energy (31.2 kcal mol^{-1}) than the square-pyramidal isomer $\mathbf{5}^{Br}_{hex}\mathbf{M}$. This type of isomer could not be located for the anti-Markovnikov regioisomer. For both regiochemistries, the N–H···Br interaction persists from the starting hydride complex $\mathbf{5}^{Br}_{hex}$ through the transition state $\mathbf{TS2}^{Br}_{hex}$ and is still found in the product $\mathbf{6}^{Br}_{hex}$. The hydroamination product, *N*-1- or *N*-2-hexylaniline, is weakly bonded to the Pt center through the C–H bond and can rearrange to yield a complex with an N-bonded hydroamination product, $\mathbf{7}^{Br}_{hex}$, shown again in Figure 10 for both regiochemistries. The Markovnikov pathway has the lower-energy transition state and σ-complex, but the rearrangement to the N-bonded complex switches the relative energy order, the anti-Markovnikov product becoming now the preferred regioisomer.

The two competitive pathways are compared in the energy diagram of Figure 11. Like for the hydroamination of ethylene,

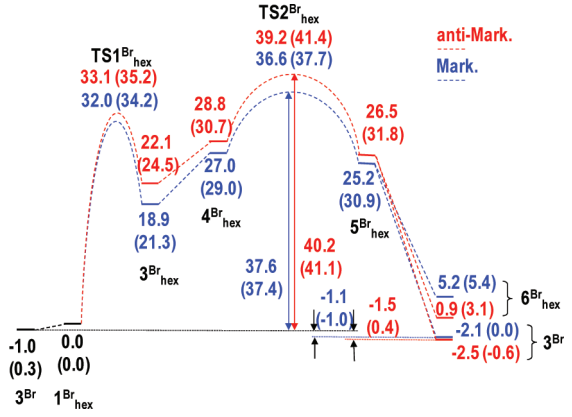

Figure 11. Relative Gibbs free energy pathways for the $PtBr_2/Br^-$-catalyzed hydroamination of 1-hexene. Values are ΔG^{CPCM} (aniline) in kcal mol^{-1} relative to $[PtBr_3(1\text{-hexene})]^-$ ($\mathbf{1}^{Br}_{hex}$) at 298.15 K (and at 423.15 K in parentheses).

the calculation shows that the TOF-determining transition state is that of the reductive elimination process forming the C–H bond between the aminoalkyl and hydride ligands. The nucleophilic addition step occurs with a transition state $\mathbf{TS1}^{Br}_{hex}$ at lower energy. Therefore, the different energy barriers at the nucleophilic addition step level have no kinetic consequence. The only interesting difference is the relative thermodynamic stability of the zwitterionic products ($\mathbf{4}^{Br}_{hex}\mathbf{M}$ is present at greater relative concentration than its isomer $\mathbf{4}^{Br}_{hex}\mathbf{A}$ under catalytic conditions). The overall rate is determined by the free energy difference between $\mathbf{TS2}^{Br}_{hex}$ and the resting state, which is calculated as *trans*-$PtBr_2(PhNH_2)_2$ (although complex $\mathbf{1}^{Br}_{hex}$ is calculated as slightly more stable at 150 °C). Because the interesting parameter here is the $\Delta\Delta G^{\ddagger}_{cycle}{}^{CPCM}$ for the two regioisomers and the resting state is shared by the two cycles, whether the resting state is *trans*-$PtBr_2(PhNH_2)_2$ or $[PtBr_3(1\text{-hexene})]^-$ (or even $[PtBr_5]^{3-}$),[55] the result does not change. From this $\Delta\Delta G^{\ddagger}_{cycle}{}^{CPCM}$ (2.6 and 3.7 kcal mol^{-1} at 298.15 and 423.15 K, respectively) an expected M/A ratio of 98.8:1.2 can be predicted at both temperatures (the greater energy difference at the higher temperature is balanced off exactly by the different *RT* term), which can be considered in qualitatively good agreement with the observed 95:5 ratio.[28]

In conclusion for this section, the results of the calculations based on the previously proposed mechanism[39] are in agreement with a number of experimental observations. (i) The catalytic activity for the hydroamination of 1-hexene (TON = 37)[27] is lower than that for ethylene (TON = 92)[26] under the same conditions, consistent with a greater $\Delta G^{\ddagger}_{cycle}$ in the former case. The difference between the two barriers at 150 °C (37.7 kcal mol^{-1} for the Markovnikov addition to 1-hexene and 35.6 kcal mol^{-1} for addition to ethylene) is actually too large to justify such a small activity difference, but it is in the right direction. Besides computational errors, a possible reason leading to an artificially smaller activity difference is a faster catalyst degradation in the presence of ethylene relative to 1-

dx.doi.org/10.1021/om2009149 | *Organometallics* 2012, 31, 294–305

hexene, but this does not seem likely on the basis of the considerations already made above. (ii) The catalytic activity for addition to 1-hexene is greater for the Markovnikov addition mode, with the calculated $\Delta\Delta G^{CPCM}$ qualitatively agreeing with the observed 95:5 ratio.

2. Halide Effect. Like for the aniline addition to ethylene, we applied the computational approach to analyze the $\Delta G^{\ddagger}_{cycle}$ for the addition of aniline to 1-hexene catalyzed by different PtX_2/X^- systems. Calculation of the various $[PtX_3(1\text{-hexene})]^-$ ($\mathbf{1}^{X}_{hex}$) and comparison with the *trans*-$PtX_2(PhNH_2)_2$ ($\mathbf{3}^{X}$) systems already discussed above reveal that the lowest-energy system (resting state) is the former for X = F and the latter for the other three halogens (see Figure 12). The much greater

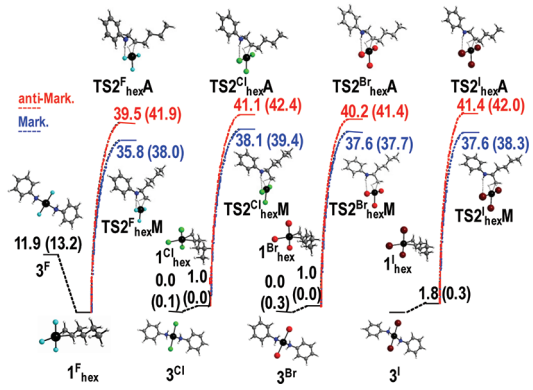

Figure 12. Relative Gibbs free energies for systems $[PtX_3(1\text{-hexene})]^-$ ($\mathbf{1}^{X}_{hex}$), *trans*-$PtX_2(PhNH_2)_2$ ($\mathbf{3}^{X}$), and the transition states of the rate-determining C−H reductive elimination steps ($\mathbf{TS2}^{X}_{hex}$) for both Markovnikov and anti-Markovnikov products related to the PtX_2/X^--catalyzed hydroamination of 1-hexene. Values are ΔG^{CPCM} (aniline) in kcal mol^{-1} relative to the resting state in each case, at 298.15 K (and at 423.15 K in parentheses).

stabilization of $\mathbf{1}^{X}_{hex}$ relative to $\mathbf{3}^{X}$ for the fluoride system can be rationalized in the same way as that of $\mathbf{1}^{X}$, since the Pt−C_2H_4 and Pt−hexene bonds have similar constitutions.

The ΔG^{CPCM} values of the TOF-determining transition state for the two regiochemistries, $\mathbf{TS2}^{X}_{hex}\mathbf{M}$ and $\mathbf{TS2}^{X}_{hex}\mathbf{A}$, are also reported in Figure 12 relative to the resting state. The $\Delta G^{CPCM}(\mathbf{TS2}^{X}_{hex}\mathbf{M}) - \Delta G^{CPCM}(\mathbf{TS2}^{X}_{hex}\mathbf{A})$ value is approximately constant (between 2.6 kcal mol^{-1} for the Br system and 3.8 kcal mol^{-1} for the I system), in agreement with a small effect of the halide nature on the M/A ratio. When considering only the heavier halides, the $\Delta G^{\ddagger}_{cycle}$ for the main (Markovnikov) pathway is greater for the Cl system, and smaller and essentially identical for the Br and I systems, whereas the iodide system was experimentally found to yield a greater TON. As already concluded above in sections 2a−2c, the experimental result is largely affected by the rate at which the catalyst decomposes, whereas the computational limitations and approximations make the $\Delta G^{\ddagger}_{cycle}$ differences between the different halide systems little reliable. Hence, a perfect match between the trends in $\Delta G^{\ddagger}_{cycle}$ and the observed TON is not to be expected. The results of the calculations qualitatively fit with the observation of a relatively halide-independent M/A regioselectivity, but a finer analysis of such small effects is probably meaningless.

3. CONCLUSIONS

Application of the catalytic mechanism recently established by a DFT study for the $PtBt_2/Br^-$-catalyzed N−H addition of aniline to ethylene[39] has provided the following results: (i) the activation barrier ($\Delta G^{\ddagger}_{cycle}$) for the $C_2H_4/PhNH_2$ reaction catalyzed by PtX_2/X^- is similar for Br, Cl, and I, though marginally smaller for the Br system, which affords the highest activity; (ii) the $\Delta G^{\ddagger}_{cycle}$ slightly increases as the aniline basicity increases (*p*-chloroaniline < aniline < *p*-methoxyaniline); (iii) the $\Delta G^{\ddagger}_{cycle}$ for the 1-hexene/$PhNH_2$ reaction is slightly greater than that for the $C_2H_4/PhNH_2$ reaction; (iv) $\Delta G^{\ddagger}_{cycle}$ for the Markovnikov addition of aniline to 1-hexene is lower than that for the anti-Markovnikov addition; and (v) the $\Delta\Delta G^{\ddagger}_{cycle}$ (M/A) for the 1-hexene/$PhNH_2$ reaction is relatively halide-independent. Some of these results are in reasonable agreement, at least qualitatively, with the experimental evidence (notably, the marked preference for the Markovnikov addition), whereas others are less reliable or in fortuitous agreement because of the small computed differences where the computational errors may not perfectly cancel out,[56,57] and because the observed trends in catalytic activity for the previously published studies (expressed by the TON) are affected by catalyst decomposition, which may not systematically be in direct relation with the turnover frequency.

Overall, it seems that all the available experimental results for the Pt-catalyzed olefin hydroamination are reasonably well rationalized by the proposed mechanism (Figure 1),[39] after allowance is made for the base-induced catalyst decomposition. For instance, decomposition seems to negatively affect the catalytic performance in the presence of fluoride ions, contrary to the computational prediction. The mechanism of Figure 1 may be considered a good basis for further mechanistic elaborations and catalyst design, which also requires, however, a fuller understanding of the catalyst degradation mechanism.

Additional studies into the catalyst degradation, learning how to prevent it or retard it, are warranted. It is also interesting to conceive other coordination geometries allowing a $\Delta G^{\ddagger}_{cycle}$ reduction, namely, a reduction of the free energy difference between the resting state and the transition state of the TOF-determining C−H reductive elimination step. Work in these directions is currently ongoing.

4. EXPERIMENTAL SECTION

a. Computational Details. All geometry optimizations were carried out by the DFT approach with the Gaussian 03 suite of programs[58] using the B3LYP functional.[59−61] All atoms except Pt and I were described by the standard 6-31+G* basis set, which includes both polarization and diffuse functions that are necessary to allow angular and radial flexibility to the highly anionic systems. The I atom was described by the LANL08d basis and the Pt atom by the LANL2TZ(f) basis, which are uncontracted versions of LANL2DZ and include an ECP.[62] The I basis set contains a d polarization and a diffuse function and the Pt basis set contains an f polarization function. The geometry optimizations were carried out on isolated molecules in the gas phase. Transition states were optimized using the synchronous transit-guided quasi-Newton (STQN) method in the gas phase. Frequency calculations were carried out for all optimized geometries in order to verify their nature as local minima, for the calculation of thermodynamic parameters at 298.15 K and at 423.15 K under the ideal gas and harmonic approximations, and for the identification of all transition states (one imaginary frequency). Solvent effects were introduced by means of C-PCM[63,64] single-point calculations on the gas-phase optimized geometries in aniline (ε = 6.89), which was considered to best approximate the reaction solvent. The solvent cavity was created by a series of overlapping spheres by the default

dx.doi.org/10.1021/om2009149 | *Organometallics* 2012, 31, 294−305

UA0 model (or SPHEREONH for the delocalized proton atoms), and all standard settings as implemented in Gaussian 03 were used for the C-PCM calculations. The reaction free energy changes in solution were calculated as $\Delta G_{solut} = \Delta G_{gas} + \Delta(\Delta G_{solv})$ and corrected for the change of standard state from the gas phase (1 atm) to solution (1 M).[65] The approach of optimizing the geometries in the gas phase and then keeping the geometry frozen for the C-PCM calculation was preferred because of convergence problems of the geometry optimization in the presence of the C-PCM, especially for molecules containing weak interactions (i.e., hydrogen bonds).

b. Catalytic Runs. *1. Yield vs Time Monitoring.* Catalytic experiments were conducted in a 100 mL stainless steel autoclave without a glass liner under magnetic stirring. In a typical procedure, the autoclave was charged with $PtBr_2$ (0.26 mmol) and the appropriate salt additive (2.6 mmol), closed, and submitted to vacuum/argon cycles. Aniline (8.3 mL, 90 mmol) was added to the autoclave by a syringe through a valve equipped with a septum and the ethylene pressure adjusted to 25 bar (ca. 100 mmol). The temperature was then raised to 150 °C. Samples were withdrawn at regular time intervals, treated with the external standard (*N*,*N*-dibutylaniline), and extracted with diethyl ether. The organic layer was analyzed by GC.

2. In the Presence of Added Base. In a typical procedure, K_2PtCl_4 (0.13 mmol) and NaBr (19.5 mmol) were introduced in the autoclave, which was then closed and submitted to vacuum/argon cycles. Subsequently, water (15 mL), aniline (4.15 mL, 45 mmol), and additional base (1.3 mmol) were added to the autoclave by a syringe through a valve equipped with a septum, and the ethylene pressure was adjusted to 25 bar (ca. 100 mmol). The temperature was then raised to 150 °C. After 10 h, the autoclave was allowed to cool to room temperature and slowly vented. The entire reaction mixture was treated with the external standard (*N*,*N*-dibutylaniline) and extracted with dichloromethane (ca. 60 mL). The organic layer was analyzed by GC.

■ ASSOCIATED CONTENT

Supporting Information

MO contour plots of all orbitals shown in Figure 3 and Cartesian coordinates for all new optimized structures. This material is available free of charge via the Internet at http://pubs.acs.org.

■ AUTHOR INFORMATION

Corresponding Author

*Fax: (+) 33-561553003. E-mail: rinaldo.poli@lcc-toulouse.fr.

■ ACKNOWLEDGMENTS

We are grateful to the ANR (Agence Nationale de la Recherche, Grant No. NT09_442499), to the CNRS (Centre National de la Recherche Scientifique), and to the IUF (Institut Universitaire de France) for support of this work. This work was granted access to the HPC resources of CINES under the allocation 2010-086343 made by GENCI (Grand Equipement National de Calcul Intensif) and to the resources of the CICT (Centre Interuniversitaire de Calcul de Toulouse, project CALMIP). P.A.D. thanks the MENESR (Ministère de l'Éducation Nationale, de l'Enseignement Supérieur et de la Recherche, France) for a Ph.D. fellowship.

■ REFERENCES

(1) Müller, T. E.; Hultzsch, K. C.; Yus, M.; Foubelo, F.; Tada, M. *Chem. Rev.* **2008**, *108*, 3795−3892.
(2) Haggins, J. *Chem. Eng. News* **1993**, *71*, 23−27.
(3) Brunet, J.-J.; Neibecker, D. In *Catalytic Heterofunctionalization*; Togni, A., Grützmacher, H., Eds.; VCH: Weinheim, Germany, 2001; pp 91−141.
(4) Borman, S. *Chem. Eng. News* **2004**, *82*, 42−43.
(5) Khedkar, V.; Tillack, A.; Benisch, C.; Melder, J. P.; Beller, M. *J. Mol. Catal. A* **2005**, *241*, 175−183.
(6) Ryu, J. S.; Li, G. Y.; Marks, T. J. *J. Am. Chem. Soc.* **2003**, *125*, 12584−12605.
(7) Hong, S.; Marks, T. J. *Acc. Chem. Res.* **2004**, *37*, 673−686.
(8) Yang, L.; Xu, L. W.; Zhou, W.; Gao, Y. H.; Sun, W.; Xia, C. G. *Synlett* **2009**, 1167−1171.
(9) Gardner, D. M.; Clark, R. T. U.S. Patent 4,454,321, 1984.
(10) Gardner, D. M.; Clark, R. T. European Patent 39,061, 1981.
(11) Schaffrath, H.; Keim, W. *J. Mol. Catal. A* **2001**, *168*, 9−14.
(12) Yi, C. S.; Yun, S. Y. *Org. Lett.* **2005**, *7*, 2181−2183.
(13) Krukowka, E.; Taube, R.; Steinborn, D. DD Patent 296,909, 1991.
(14) Coulson, D. R. *Tetrahedron Lett.* **1971**, 429−430.
(15) Coulson, D. R. U.S. Patent 3,758,586, 1973.
(16) Diamond, S. E.; Mares, F.; Szalkiewicz, A. *Fundam. Res. Homogeneous Catal.* **1979**, *3*, 345−358.
(17) Diamond, S. E.; Mares, F. U.S. Patent 4,215,218, 1980.
(18) Giner, X.; Najera, C. *Synlett* **2009**, 3211−3213.
(19) Liu, X. Y.; Li, C. H.; Che, C. M. *Org. Lett.* **2006**, *8*, 2707−2710.
(20) Zhang, J. L.; Yang, C. G.; He, C. *J. Am. Chem. Soc.* **2006**, *128*, 1798−1799.
(21) Zhang, Z. B.; Lee, S. D.; Widenhoefer, R. A. *J. Am. Chem. Soc.* **2009**, *131*, 5372−5373.
(22) Giner, X.; Najera, C. *Org. Lett.* **2008**, *10*, 2919−2922.
(23) Wang, X.; Widenhoefer, R. A. *Organometallics* **2004**, *23*, 1649−1651.
(24) Karshtedt, D.; Bell, A. T.; Tilley, T. D. *J. Am. Chem. Soc.* **2005**, *127*, 12640−12646.
(25) McBee, J. L.; Bell, A. T.; Tilley, T. D. *J. Am. Chem. Soc.* **2008**, *130*, 16562−16571.
(26) Brunet, J. J.; Cadena, M.; Chu, N. C.; Diallo, O.; Jacob, K.; Mothes, E. *Organometallics* **2004**, *23*, 1264−1268.
(27) Brunet, J. J.; Chu, N. C.; Diallo, O. *Organometallics* **2005**, *24*, 3104−3110.
(28) Rodriguez-Zubiri, M.; Anguille, S.; Brunet, J.-J. *J. Mol. Catal. A* **2007**, *271*, 145−150.
(29) Brunet, J.-J.; Chu, N.-C.; Rodriguez-Zubiri, M. *Eur. J. Inorg. Chem.* **2007**, 4711−4722.
(30) Jeffery, T. *Tetrahedron* **1996**, *52*, 10113−10130.
(31) Amatore, C.; Jutand, A. *J. Organomet. Chem.* **1999**, *576*, 254−278.
(32) Handy, S. T.; Okello, M. *Tetrahedron Lett.* **2003**, *44*, 8395−8397.
(33) Maitlis, P. M.; Haynes, A.; James, B. R.; Catellani, M.; Chiusoli, G. P. *Dalton Trans.* **2004**, 3409−3419.
(34) Senn, H. M.; Blochl, P. E.; Togni, A. *J. Am. Chem. Soc.* **2000**, *122*, 4098−4107.
(35) Tsipis, C. A.; Kefalidis, C. E. *J. Organomet. Chem.* **2007**, *692*, 5245−5255.
(36) Kovacs, G.; Ujaque, G.; Lledós, A. *J. Am. Chem. Soc.* **2008**, *130*, 853−864.
(37) Kovacs, G.; Lledos, A.; Ujaque, G. *Organometallics* **2010**, *29*, 5919−5926.
(38) Vo, L. K.; Singleton, D. A. *Org. Lett.* **2004**, *6*, 2469−2472.
(39) Dub, P. A.; Poli, R. *J. Am. Chem. Soc.* **2010**, *132*, 13799−13812.
(40) Dub, P. A.; Rodriguez-Zubiri, M.; Daran, J.-C.; Brunet, J.-J.; Poli, R. *Organometallics* **2009**, *28*, 4764−4777.
(41) Poli, R. *Comments Inorg. Chem.* **2009**, *30*, 177−228.
(42) Kozuch, S.; Shaik, S. *Acc. Chem. Res.* **2011**, *44*, 101−110.
(43) Dub, P. A.; Poli, R. *J. Mol. Catal. A* **2010**, *324*, 89−96.
(44) Caulton, K. G. *New J. Chem.* **1994**, *18*, 25−41.
(45) Drago, R. S.; Wong, N. M. *Inorg. Chem.* **1995**, *34*, 4004−4007.
(46) Liu, G.-H.; Parr, R. G. *J. Am. Chem. Soc.* **1995**, *117*, 3179−3188.
(47) Pearson, R. G. *Coord. Chem. Rev.* **1990**, *100*, 403−425.
(48) Dub, P. A.; Rodriguez-Zubiri, M.; Baudequin, C.; Poli, R. *Green Chem.* **2010**, 1392−1396.
(49) Dorta, R.; Egli, P.; Zurcher, F.; Togni, A. *J. Am. Chem. Soc.* **1997**, *119*, 10857−10858.

(50) Pryadun, R.; Sukumaran, D.; Bogadi, R.; Atwood, J. D. *J. Am. Chem. Soc.* **2004**, *126*, 12414−12420.
(51) Balacco, G.; Natile, G. *J. Chem. Soc., Dalton Trans.* **1990**, 3021−3024.
(52) Al-Najjar, I. M.; Green, M. *J. Chem. Soc., Dalton Trans.* **1979**, 1651−1656.
(53) (a) Dub, P. A.; Daran, J.-C.; Levina, V. A.; Belkova, N. V.; Shubina, E. S.; Poli, R. *J. Organomet. Chem.* **2011**, *696*, 1174−1183. (b) Dub, P. A.; Béthegnies, A.; Poli, R. *Eur. J. Inorg. Chem.* **2011**, 5167−5172.
(54) Landini, D.; Maia, A.; Rampoldi, A. *J. Org. Chem.* **1989**, *54*, 328−332.
(55) Aullón, G.; Gómez, K.; González, G.; Jansat, S.; Martínez, M.; Poli, R.; Rodríguez-Zubiri, M. *Inorg. Chem.* **2011**, *50*, 5628−5636.
(56) Wheeler, S. E.; Moran, A.; Pieniazek, S. N.; Houk, K. N. *J. Phys. Chem. A* **2009**, *113*, 10376−10384.
(57) Pieniazek, S. N.; Clemente, F. R.; Houk, K. N. *Angew. Chem., Int. Ed.* **2008**, *47*, 7746−7749.
(58) Frisch, M. J.; Trucks, G. W.; Schlegel, H. B.; Scuseria, G. E.; Robb, M. A.; Cheeseman, J. R.; Montgomery, J. A., Jr.; Vreven, T.; Kudin, K. N.; Burant, J. C.; Millam, J. M.; Iyengar, S. S.; Tomasi, J.; Barone, V.; Mennucci, B.; Cossi, M.; Scalmani, G.; Rega, N.; Petersson, G. A.; Nakatsuji, H.; Hada, M.; Ehara, M.; Toyota, K.; Fukuda, R.; Hasegawa, J.; Ishida, M.; Nakajima, T.; Honda, Y.; Kitao, O.; Nakai, H.; Klene, M.; Li, X.; Knox, J. E.; Hratchian, H. P.; Cross, J. B.; Adamo, C.; Jaramillo, J.; Gomperts, R.; Stratmann, R. E.; Yazyev, O.; Austin, A. J.; Cammi, R.; Pomelli, C.; Ochterski, J. W.; Ayala, P. Y.; Morokuma, K.; Voth, G. A.; Salvador, P.; Dannenberg, J. J.; Zakrzewski, V. G.; Dapprich, S.; Daniels, A. D.; Strain, M. C.; Farkas, O.; Malick, D. K.; Rabuck, A. D.; Raghavachari, K.; Foresman, J. B.; Ortiz, J. V.; Cui, Q.; Baboul, A. G.; Clifford, S.; Cioslowski, J.; Stefanov, B. B.; Liu, G.; Liashenko, A.; Piskorz, P.; Komaromi, I.; Martin, R. L.; Fox, D. J.; Keith, T.; Al-Laham, M. A.; Peng, C. Y.; Nanayakkara, A.; Challacombe, M.; Gill, P. M. W.; Johnson, B.; Chen, W.; Wong, M. W.; Gonzalez, C.; Pople, J. A. *Gaussian 03*, revision C.02; Gaussian, Inc.: Wallingford, CT, 2004.
(59) Becke, A. D. *J. Chem. Phys.* **1993**, *98*, 5648−5652.
(60) Lee, C. T.; Yang, W. T.; Parr, R. G. *Phys. Rev. B* **1988**, *37*, 785−789.
(61) Miehlich, B.; Savin, A.; Stoll, H.; Preuss, H. *Chem. Phys. Lett.* **1989**, *157*, 200−206.
(62) Roy, L. E.; Hay, P. J.; Martin, R. L. *J. Chem. Theory Comput.* **2008**, *4*, 1029−1031.
(63) Barone, V.; Cossi, M. *J. Phys. Chem. A* **1998**, *102*, 1995−2001.
(64) Cossi, M.; Rega, N.; Scalmani, G.; Barone, V. *J. Comput. Chem.* **2003**, *24*, 669−681.
(65) Winget, P.; Cramer, C. J.; Truhlar, D. G. *Theor. Chem. Acc.* **2004**, *112*, 217−227.